CrossMark

The F-actin modifier villin regulates insulin granule dynamics and exocytosis downstream of islet cell autoantigen 512

Hassan Mziaut [1,2], Bernard Mulligan [1,2], Peter Hoboth [1,2], Oliver Otto [3], Anna Ivanova [1,2], Maik Herbig [3], Desiree Schumann [4], Tobias Hildebrandt [4], Jaber Dehghany [5], Anke Sönmez [1,2], Carla Münster [1,2], Michael Meyer-Hermann [5], Jochen Guck [3], Yannis Kalaidzidis [6], Michele Solimena [1,2,6,*]

ABSTRACT

Objective: Insulin release from pancreatic islet β cells should be tightly controlled to avoid hypoglycemia and insulin resistance. The cortical actin cytoskeleton is a gate for regulated exocytosis of insulin secretory granules (SGs) by restricting their mobility and access to the plasma membrane. Prior studies suggest that SGs interact with F-actin through their transmembrane cargo islet cell autoantigen 512 (Ica512) (also known as islet antigen 2/Ptprn). Here we investigated how Ica512 modulates SG trafficking and exocytosis.
Methods: Transcriptomic changes in *Ica512*$^{-/-}$ mouse islets were analyzed. Imaging as well as biophysical and biochemical methods were used to validate if and how the *Ica512*-regulated gene *villin* modulates insulin secretion in mouse islets and insulinoma cells.
Results: The F-actin modifier *villin was* consistently downregulated in *Ica512*$^{-/-}$ mouse islets and in *Ica512*-depleted insulinoma cells. Villin was enriched at the cell cortex of β cells and dispersed *villin*$^{-/-}$ islet cells were less round and less deformable. Basal mobility of SGs in *villin*-depleted cells was enhanced. Moreover, in cells depleted either of *villin* or *Ica512* F-actin cages restraining cortical SGs were enlarged, basal secretion was increased while glucose-stimulated insulin release was blunted. The latter changes were reverted by overexpressing villin in *Ica512*-depleted cells, but not *vice versa*.
Conclusion: Our findings show that villin controls the size of the F-actin cages restricting SGs and, thus, regulates their dynamics and availability for exocytosis. Evidence that villin acts downstream of *Ica512* also indicates that SGs directly influence the remodeling properties of the cortical actin cytoskeleton for tight control of insulin secretion.

1. INTRODUCTION

Regulated exocytosis is a fundamental cellular process that involves the release of stored secretory cargos from membranous vesicles into the extracellular space. In pancreatic islet β cells, newly synthesized insulin-containing secretory granules (SGs) are formed at the trans-Golgi network and are transported to the cell cortex for preferential glucose-stimulated exocytosis relative to older SGs [1,2]. The initial phase of vesicle transport is microtubule-dependent, while both microtubules and the cortical F-actin network regulate the motility and access of SGs to the plasma membrane and their release in response to stimuli only. The exocytosis of SGs is facilitated by drugs, which depolymerize microfilaments [3–6], and is inhibited by drugs, which promote polymerization [3,7], although high concentrations of F-actin disrupting drugs can also inhibit exocytosis [4]. Hence, the actin cytoskeleton has a complex role in regulating insulin release, but its precise molecular links with SGs remain undefined. Importantly, altered insulin secretion causes type 2 diabetes. Thus, improving our understanding of how the cytoskeleton controls insulin secretion could enable us to identify additional approaches to treat this disease.
We previously reported that the islet cell autoantigen 512 (Ica512; also known as Ia-2 and Ptprn) tethers insulin SGs to actin

microfilaments via its association to the adapter protein β2-syntrophin [8—10]. Ica512 is an atypical member of the receptor protein-tyrosine phosphatase family with a single cytosolic PTP domain, which lacks protein phosphatase activity. It is mostly expressed in neuroendocrine cells, where it is selectively enriched in the SG membrane. Genetic deletion of *Ica512* in mice is associated with mild glucose intolerance and decreased glucose-responsive insulin secretion [9—12]. To gain further insight into how Ica512 regulates insulin secretion, we anaylzed the gene expression profile of *Ica512*-depleted mouse islets. We show that *Ica512* depletion leads to downregulation of the F-actin modifier *villin* in β cells, thereby increasing the size of actin cages surrounding cortical SGs and thus their motility and exocytosis in basal conditions, while reducing glucose-stimulated insulin release.

2. MATERIALS AND METHODS

2.1. Culture of mouse islets and insulinoma MIN6 and INS-1 cells
The whole body knockout mice *Ica*512 [13] and *villin* [14] were generated as previously described. Pancreatic islets were isolated from 8 to 17-week-old *Ica512*−/− mice and 8 to 44-week-old *villin*−/− mice and wild type littermates and were cultured for 24 h before subsequent experiments. All animal protocols were approved by the institutional animal care and use committee and all experiments were performed in accordance with relevant guidelines and regulations. Mouse MIN6 and rat INS-1 insulinoma cells were kind gifts from Dr. Jun-ichi Miyazaki (Osaka University, Japan) and C. Wollheim (University of Geneva, Switzerland), respectively, and were grown in six-well plates as previously described [15,16].

2.2. Transcriptomic profiling of mouse islets
Total RNA was isolated from the islets of 12-week-old wild-type and *Ica512*−/− mice (7 mice/group) using RNeasy (Qiagen, Hilden, Germany). For microarray analysis, 350 ng of islet RNA was amplified with the Illumina® Total Prep RNA Amplification Kit (Ambion, Inc., Austin, Tx) and cRNA was labeled with biotin-UTP. Then, 700 ng of labeled-cRNAs in 15 μL for each hybridization was dispensed on Sentrix MouseRef-8v2 Expression BeadChips (Illumina Inc., San Diego, CA). After hybridization (16 h, 58 °C), the arrays were washed according to the manufacturer's instructions (Illumina Inc.). The arrays were stained with streptavidin—cyanine-3, and scanned with the BeadArray Reader for quantification. For transcriptomic profiling using Agilent chips, total RNA from islets of 12-week-old wild-type and *Ica512*−/− mice (7 mice/group) was isolated as described above. Cyanine-3-labeled cRNA was prepared and hybridized onto 4 × 44K Whole Mouse Genome microarrays (AMADID 14868) from 0.6 μg of total RNA using the One-Color Microarray-Based Gene Expression Analysis v5.5 protocol (Agilent, Santa Clara, CA). Slides were scanned on an Agilent DNA Microarray Scanner (G2505C), and the data were extracted using Agilent Feature Extraction Software (version 10.0). Data analysis was done with Agilent GeneSpring software (version 11.0) with scale to median normalization of all samples and no baseline transformation. For strand-specific RNA sequencing, the library was prepared as previously described [17]. Sample libraries were pooled for 75-bp single end sequencing on an Illumina HiSeq 2000 (Illumina Inc.), resulting in approximately 30 million reads per sample. Alignment of the reads to the mm9 transcriptome was performed with pBWA [18]. Tests for differential gene expression were performed with DESeq [19]. *P* values for the statistical significance of the fold change were adjusted for multiple testing using the Benjamini—Hochberg method to control the false discovery rate [20].

2.3. cDNA constructs and siRNA oligonucleotides
The plasmid pEGFP-N1 was used to induce the expression of enhanced green fluorescent protein (EGFP; Clontech, Foster City, CA). The plasmids used to induce the expression of human *Ica512-GFP* and *insulin-SNAP* have been described elsewhere [21,22]. The cDNA of mouse *villin* (IMAGE: 4236751) was cloned as an *Ecorl-Agel* insert into pEGFP-N1 using the oligonucleotides indicated in the supplementary material. The synthetic small interfering RNA (siRNA) oligonucleotides targeting mouse and rat *Ica512* as well as mouse and rat *villin* (see Supplementary Table 1) were purchased from Riboxx (Radebeul, Germany) using the Elbashir algorithm [23].

2.4. Glucose and insulin tolerance tests
Oral, intraperitoneal, and intravenous glucose tolerance tests (OGTT, IPGTT, and IVGTT) were done on C57BL/6 wild-type and *villin*−/− mice after an overnight fast. Glucose (1 g/kg) was given orally, intraperitoneally, or intravenously at 0 min. For the insulin tolerance test, mice were fasted for 4 h before an injection of human regular insulin (0.75 U/kg). Tail blood glucose levels were measured at the indicated times with the Bayer Elite glucometer (Bayer, Leverkusen, Germany).

2.5. Transfection of islets and insulinoma cells, and measurement of insulin secretion
Silencing of *villin* in mouse islets was performed 1 day after isolation using 100 nM of siRNA and DOTAP as the transfection reagent (Roche, Basel, Switzerland). After 2 days, the islets were harvested for western blotting or incubated in resting buffer with 5.5 mM glucose for 1 h and then either kept at rest or stimulated with 16.7 mM glucose for 1.5 h, and insulin secretion was measured using a radioimmunoassay (Merck Millipore, Billerica, MA).
For RNAi-mediated knockdown of *Ica512* or *villin*, insulinoma cells were transfected 1 day after seeding with the respective siRNAs (*Ica512* siRNA, 50 nM; *villin* siRNA, 75 nM; scramble siRNA, 50—75 nM) using Dharmafect reagent (2.5 μL/well) (GE Dharmacon, Lafayette, CO). Three days later, cells were harvested for RNA extraction, western blotting, confocal imaging, or measurement of glucose-stimulated insulin secretion. For measurement of glucose-stimulated insulin secretion, cells were transferred to growth media containing 2.8 mM glucose for 1 h, then for 1 h in resting buffer also with 2.8 mM glucose, and then kept at rest or stimulated with 25 mM glucose for 1.5 h. Insulin content and release were measured using the AlphaLisa kit (Thermo Fisher, Waltham, MA).
For single or combined expression of Ica512-GFP, villin-GFP, INS-SNAP and pEGFPN.1, insulinoma cells were transfected with the corresponding plasmid(s) (1.5 μg plasmid/well) by electroporation as previously described [24,25]. On day 1 post-transfection, some cells were re-treated with *Ica512*, *villin*, or scramble siRNAs, as described above.

2.6. Real-time PCR
RNA was isolated from control and *villin*-depleted MIN6 cells using the RNAeasy kit (Qiagen). Mouse *insulin1* mRNA expression was quantified by RT-PCR using specific oligonucleotides (Supplementary Table 1).

2.7. Cell extracts and western blotting
Isolated mouse islets, MIN6 and INS-1 cells were washed with ice-cold PBS and extracted in lysis buffer (10 mM Tris—HCl, pH 8.0, 140 mM NaCl, 1% Triton X-100, 1 mM EDTA, 1 mM phenylmethylsulfonyl fluoride, 1% phosphatase inhibitors [Calbiochem/Merck Millipore], and 1% protease inhibitor mixture [Sigma, St. Louis, MO]) at 4 °C. Western blotting was performed as previously described [26] using the

Original article

following primary antibodies: mouse monoclonal anti-Ica512 HM1 [26] and anti-γ-tubulin (Sigma), rabbit polyclonal anti-villin (Cell Signaling Technology, Danvers, MA), and goat polyclonal anti-GFP (Clontech). Chemiluminescence was developed and quantified as previously described [9].

2.8. Immunocytochemistry and confocal microscopy

Immunocytochemistry on pancreas tissue sections of $Ica512^{-/-}$ and $villin^{-/-}$ mice and control littermates was performed as previously described [27]. Transfected or control INS-1 cells were immunolabeled as previously described [21]. In some instances, cells were incubated in resting buffer with 2.8 mM glucose or stimulated with 25 mM glucose and 55 mM KCl for 1.5 h before being fixed. Tissue sections and cultured cells were labeled using the following primary and secondary antibodies: guinea pig anti-insulin (Abcam, Cambridge, UK), rabbit anti-villin (Cell Signaling Technology), goat anti-rabbit Alexa[568]-conjugated IgG and goat anti-guinea pig Alexa[488]-conjugated IgG (Thermo Fisher). Nuclei were counterstained with 4′,6-diamidino-2-phenylindole (Sigma), and coverslips were mounted with Mowiol (Calbiochem/Merck Millipore). Images of 0.5-μm optical tissue sections were acquired at room temperature with an inverted confocal microscope (Zeiss Axiovert 200M) equipped with a Plan-Apochromat × 63 oil objective, numerical aperture 1.4, a Zeiss LSM510 scan head with photomultiplier tubes, and Zeiss LSM 510 AIM software version 4 (Zeiss, Göttingen, Germany).

2.9. Total internal reflection fluorescence microscopy (TIRFM)

Prior to imaging, cells grown in an open chamber were incubated in resting media and transferred onto a thermostat-controlled (37 °C) stage. Insulin-SNAP[+] SGs were labeled as previously described [22] with the SNAP substrate TMR-Star (New England Biolabs, Ipswich, MA). The SGs were visualized in cells cotransfected with either EGFP or villin-GFP after treatment with the $Ica512$, $villin$, or scramble siRNAs. Videos were acquired with a Nikon microscope (Nikon, Tokyo, Japan) equiped with Andor DU-897 camera (Andor, Belfast, Rochester, NY). Pixel binning was set to 1×, multiplier to 300, read out speed to 10 MHz, and the excitation wavelength at 561 nm was set to a power of 2%. Images were collected using NIS-AR4.11.00 software (Nikon) at 30 frames/s with an exposure time of 10 ms/frame giving a total recording time of 1 min (2000 frames) for each movie. Automated image analysis was performed with MotionTracking/Kalaimoscope software (Transinsight GmbH, Dresden, Germany), as previously described [2,9]. The processive movement was defined as a motion in the same direction for at least four successive sequence frames and the percentage of processive excursions within total distance was calculated as previously described [22]. Other parameters of SG dynamics, including cumulative diffusion, mean square displacement, component analysis, and track maximum displacement were calculated as previously described [2]. The density of cortical SGs was calculated using ≥16 movies of resting or stimulated GFP[+] control and $villin$-depleted cells and of $villin$-depleted cells co-expressing villin-GFP, by using the cytosolic GFP signal to calculate the cell surface area. To estimate the size of actin cages, we analyzed the mean square displacement of the SG center within the cortical region as this approach has been shown to provide values for actin cage size that are in good agreement with those theoretically predicted [28,29]. Since the mean square displacement was measured to the saturation value, SGs could visit all available positions within the actin "cage". Accordingly, the 2D projected area of the actin cage equaled the sum of the area covered by the displacement of the SG center plus the area covered by a SG according to the following formula:

$$A_{cage} = A_{mean-square-displacement} + A_{SG}, \Rightarrow \pi \cdot S_{cage}^2$$
$$= \pi \cdot MSD + \pi \cdot S_{SG}^2$$

Where S_{cage} is the characteristic size of the actin cage, S_{SG} is the size of a SG of 125 nm radius [30], MSD is the saturation value of the SG center mean square displacement. Then $S_{cage} = \sqrt{MSD + S_{SG}^2}$.

2.10. Real-time deformability cytometry

Cell mechanical characterization was performed using real-time deformability cytometry (RT-DC) as previously described [31]. Pancreatic islets were isolated from 8 to 20-week-old $villin^{-/-}$ mice and wild-type littermates as previously described [13]. Approximately 200 islets per condition and per assay were enzmatically dispersed into single cell suspensions using accutase, centrifuged at 2000× g for 2 min and gently resuspended in PBS containing 0.5% (w/v) methylcellulose. For drug treatment, islets were treated with latrunculin A at 0.2 μM or DMSO (0.1%, v/v) 15 min before the RT-DC assay. Data analysis was performed as previously described [31]. One-dimensional linear mixed models were used to compare the size and mechanical properties independently. The experimental situation was assumed to be described by one fixed and one random effect and took into account the variation of three biological replicates.

2.11. Statistics

Statistical analyses were performed using t-tests in Microsoft Excel 12.3.6, while the ProbStudent- and Kolmogorov−Smirnov tests are included in the MotionTracking/Kalaimoscope software. The ProbStudent-t test was applied to null-hypothesis that difference between glucose disposal curves in $villin^{+/+}$ and $villin^{-/-}$ mice equals zero. Briefly, we calculated the difference between corresponding points of the curves, then we took mean and SEM of differences and calculate p_value as incomplete Beta-function I((n − 1)/2, 0.5, (n − 1)/ (n − 1 + (mean/SEM)^2), where n is number of points in curves [32]. For 12−14 weeks OGTT the following values were found: 1.366666667, 2.633333333, 0.766666667, 0.666666667, 0.966666667, 1.5. Therefore, the mean = 1.31667, the SEM 0.295365, n = 6, and the p-value = 0.00665419. For 40-40 weeks IPGTT the following values were found: 0.166666667, 3.033333333, 3.333333333, 1.633333333, 1.733333333, 2.933333333. Therefore, the mean = 2.13889, the SEM = 0.488794 (n = 6), and the p-value = 0.00718262. Since p-values are small (<<0.05), the null-hypothesis that glucose disposal curves in $villin^{+/+}$ and $villin^{-/-}$ mice have no differences was rejected. Results are presented as the mean ± standard error (SE) unless otherwise stated. Values of p < 0.05 were considered statistically significant. Bars show standard deviations from at least three independent experiments unless otherwise stated. Histograms were prepared using Microsoft Excel (Microsoft Corp., Redmond, WA).

3. RESULTS

3.1. $Ica512$ regulates the expression of $villin$ in pancreatic β cells

The gene expression profiles of islets isolated from $Ica512^{-/-}$ mice and control littermates were compared. The gene ontology analysis indicated that $villin$ was the most consistently downregulated gene in $Ica512^{-/-}$ mouse islets, with a mean decreased expression of ∼2 fold among the three transcriptomic profiling methods (Table 1). The genetic interaction between $villin$ and $Ica512$ was verified by confocal imaging of mouse $Ica512^{-/-}$ and $Ica512^{+/+}$ pancreatic cryosections immunostained for villin and insulin (Figure 1A). These

Table 1 — Transcriptomic profiling of mouse islets from *Ica512*$^{-/-}$ and control littermates.

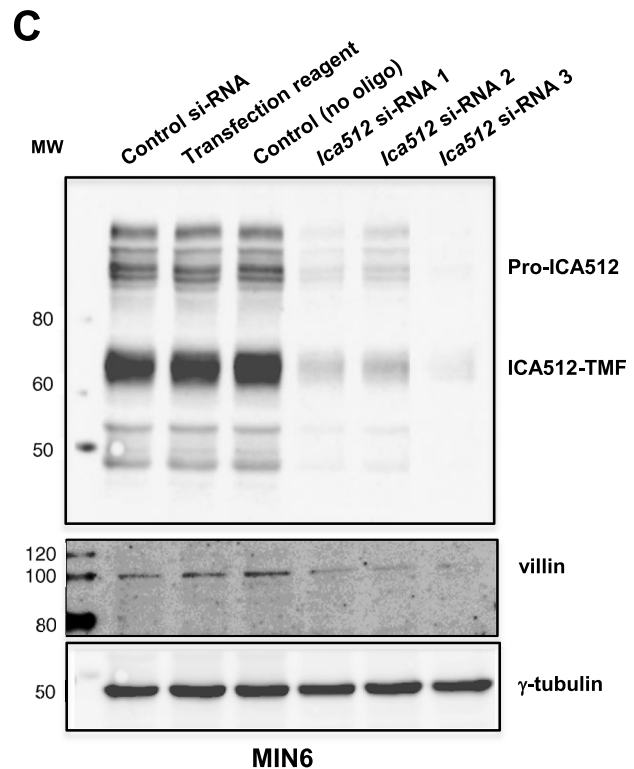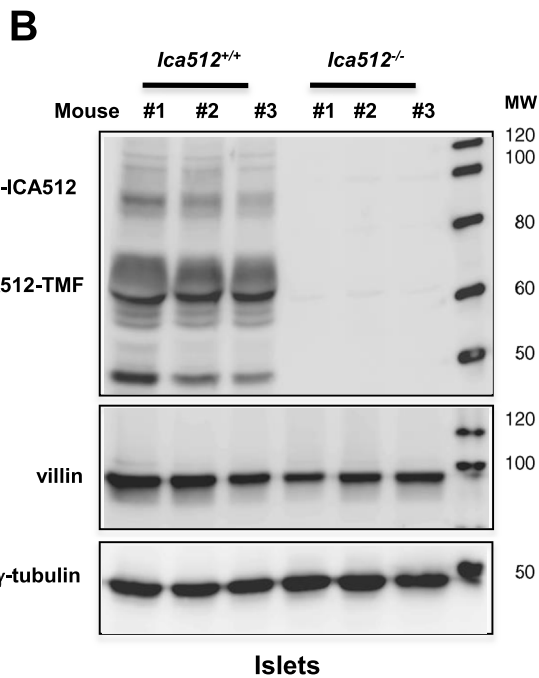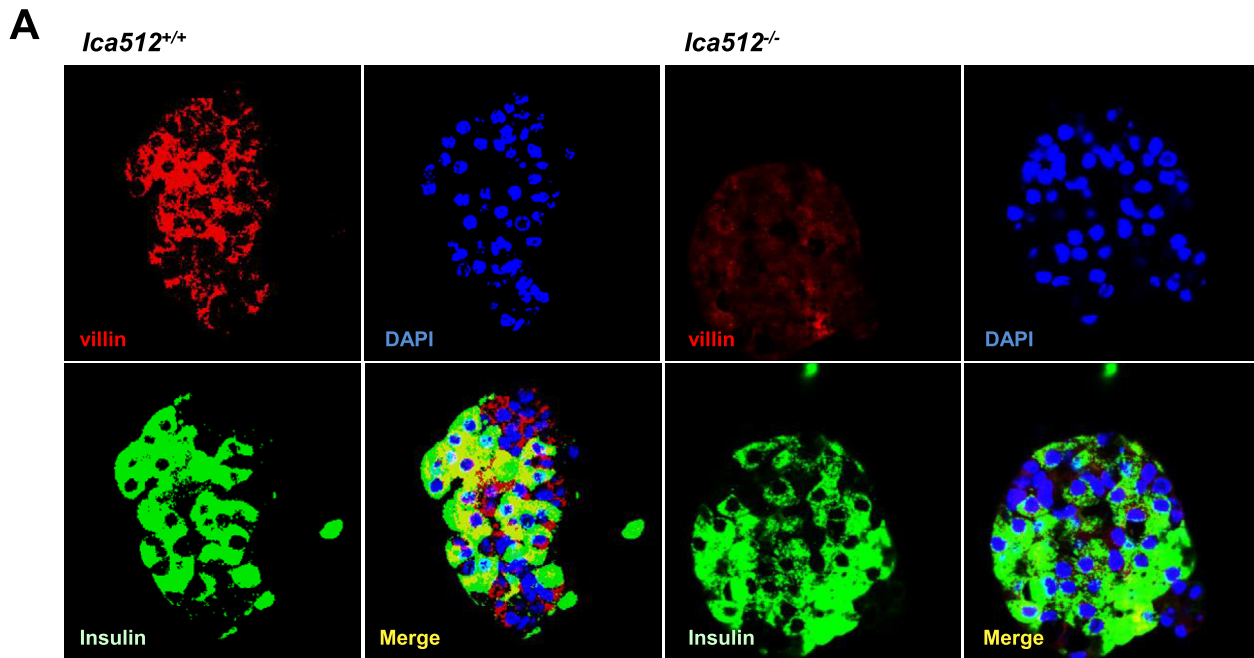| Gene name	Probe ID	Illumina			Agilent			RNA sequencing		
		Log2 fold change	p-val	Adj p-val	Log2 fold change	p-val	Adj p-val	Log2 fold change	p-val	Adj p-val
Ica512/Ptprn	ILMN_1245627	−2.98	3.20E−06	2.30E−02	−2.19	0.0000	0.0000	−4.36	4.16E−119	9.40E−115
Vil1	ILMN_2518406	−1.04	1.90E−05	6.20E−02	−1.32	0.0000	0.0000	−0.66	8.27E−05	0.05

Figure 1: Villin expression is reduced in *Ica512*$^{-/-}$ mice and *Ica512*-depleted MIN6 cells. (A) Confocal images of mouse pancreatic cryosections from *Ica512*$^{+/+}$ and *Ica512*$^{-/-}$ mice were co-stained for villin (red) and insulin (green). The nuclei were stained with DAPI (blue). **(B)** Immunoblotting for Ica512, villin, and γ-tubulin using extracts of islets isolated from *Ica512*$^{+/+}$ or *Ica512*$^{-/-}$ mice (in triplicate). **(C)** Immunoblotting for Ica512, villin, and γ-tubulin using extracts of control and *Ica512*-depleted MIN6 cells (in triplicate).

analyses showed that villin is enriched in pancreatic islet cells, including insulin$^+$ β cells, compared with pancreatic acinar cells and corroborated its downregulation in *Ica512*$^{-/-}$ islets *in situ*. Western blotting analysis also showed that its protein expression was ∼2-fold lower in *Ica512*$^{-/-}$ islets than in *Ica512*$^{+/+}$ islets (Figure 1B and Supplementary Figure 1A), consistent with the transcriptomics data. We then investigated whether acute depletion of *Ica512* affected *villin* expression in mouse MIN6 and rat INS-1 insulinoma cells; the latter cell-type expresses more villin than the former cell-type (Supplementary Figure 1B). siRNA for *Ica512* downregulated its protein expression by 90% ± 4.5% in MIN6 cells (Supplementary Figure 1C) and by 65% ± 10.4% in INS-1 cells (Supplementary Figure D,E), and that of villin by 52% ± 13.7% and 42% ± 9.6%, respectively (Figure 1C and Supplementary Figure 1F,G). Immunostaining of INS-1 cells showed that villin is enriched in the cell cortex, the typical location for an actin binding protein (Supplementary Figure 2A). Villin immunoreactivity was absent when the primary antibody was omitted and was sensitive to RNAi-mediated knockdown of *villin* (Supplementary Figure 2A,C). Accordingly, the islets from *villin*$^{-/-}$ mice were not immunoreactive for villin (Supplementary Figure 2B). Notably, villin immunoreactivity was enhanced in cells stimulated with 25 mM glucose and 55 mM KCl for 2 h (Supplementary Figure 2A), which promotes membrane depolarization and thus calcium influx. Because villin is a globular protein with an autoinhibited configuration that is released upon calcium binding [33], this observation suggests that villin changes its conformation in conditions that stimulate insulin release from β cells.

Taken together, these data indicate that the genetic association of *villin* and *Ica512* is conserved in mouse and rat. The acute downregulation of villin after silencing *Ica512* in insulinoma cells suggest that decreased expression of villin in *Ica512*$^{-/-}$ mouse islets is unlikely to be the result of a developmental adaptive process.

3.2. Role of villin in glucose homeostasis

To gain insight into the role of villin in glucose homeostasis, we performed glucose tolerance tests in *villin*$^{-/-}$ and *villin*$^{+/+}$ mice [14]. Glucose concentrations in 12—14-week-old *villin*$^{-/-}$ mice were lower (p-value of ProbStudent-test = 0.006, see Materials and Methods for details) than in *villin*$^{+/+}$ mice in the OGTT (Supplementary Figure 3A) but not in the IPGTT (p-value of ProbStudent-test = 0.110) (Supplementary Figure 3B). However, in 40—44-week-old *villin*$^{-/-}$ mice glucose concentrations were lower (p-value of ProbStudent-test = 0.007, see Materials and Methods for details) than in *villin*$^{+/+}$ mice also in the IPGTT (Figure 2B). This mild phenotype could reflect a modestly reduced glucose uptake by *villin*$^{-/-}$ intestine cells. Conversely, the IVGTT profiles of youger and older *villin*$^{-/-}$ and *villin*$^{+/}$
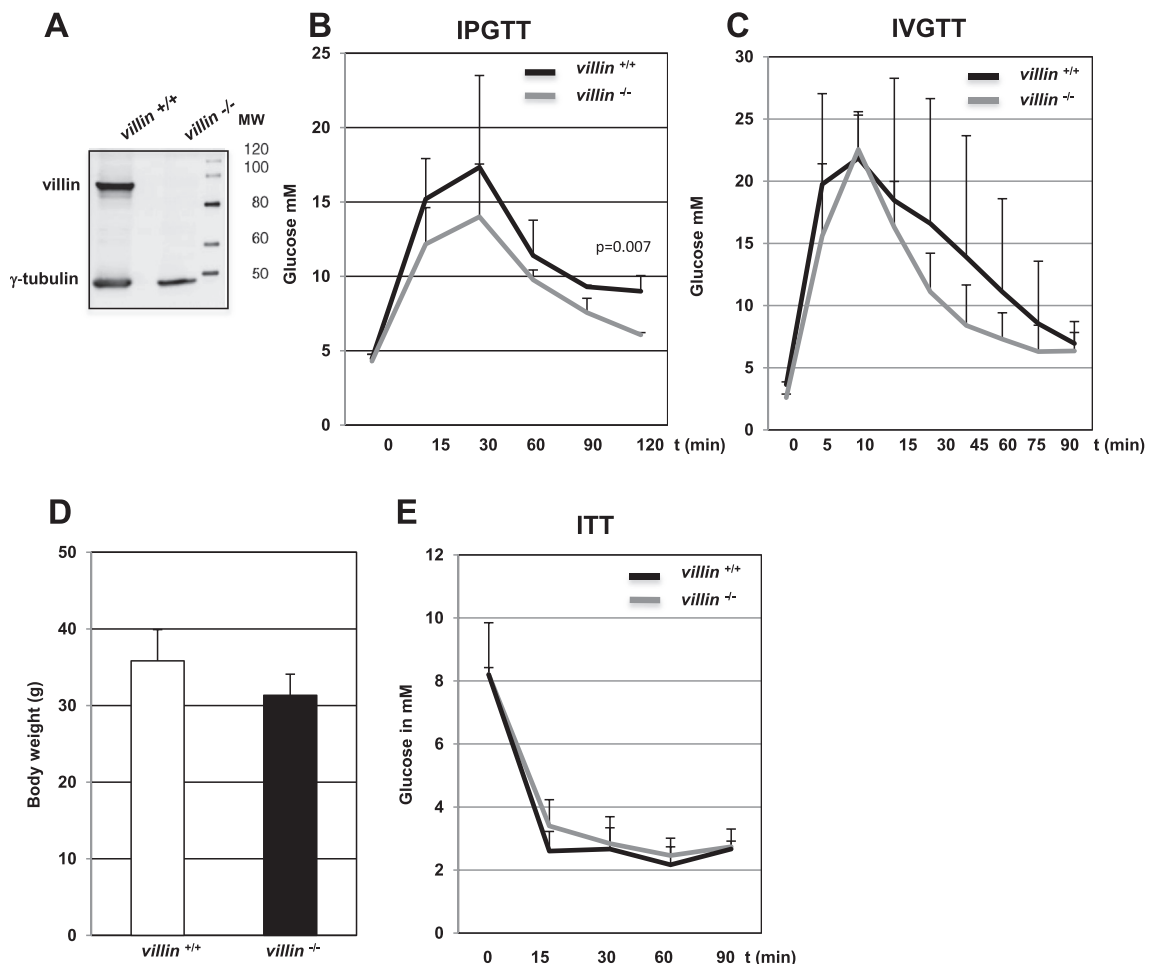

Figure 2: Glucose tolerance and insulin sensitivity of *villin*$^{-/-}$ mice. (A) Immunoblotting for villin and γ-tubulin using extracts of islets isolated from *villin*$^{+/+}$ and villin$^{-/-}$ mice. **(B,C)** Intraperitoneal **(B)** and intravenous **(C)** glucose tolerance tests in 40—44-week-old *villin*$^{+/+}$ and *villin*$^{-/-}$ mice. **(D)** Body weight of 44-week-old *villin*$^{+/+}$ and villin$^{-/-}$ mice. **(E)** Insulin tolerance tests in 44-week-old *villin*$^{+/+}$ and villin$^{-/-}$ mice.

+ mice were comparable (Figure 2C and Supplementary Figure 3C). The body weight and insulin sensitivity of *villin*$^{-/-}$ and *villin*$^{+/+}$ mice were similar (Figure 2D,E).

3.3. Villin regulates the cytoskeleton of islet cells

Next, we investigated whether villin regulates the cytoskeleton of islet β cells. To achieve this, we compared the mechanical properties of *villin*$^{-/-}$ and *villin*$^{+/+}$ dispersed islet cells by RT-DC. RT-DC allows researchers to quantify cell deformability by measuring the deviation from circularity of single cells prior and after their flow from the reservoir into a channel of variable size within a microfluidic chamber [31]. The suitability of this assay was verified by measuring the deformation of *villin*$^{+/+}$ islet cells treated with the F-actin depolymerizing agent latrunculin A or DMSO as a control. As expected, latrunculin A-treated islet cells were more deformed (i.e. less stiff) than untreated cells (Figure 3A). The size and deformation of *villin*$^{-/-}$ and

villin$^{+/+}$ islet cells in the reservoir were comparable (Figure 3B,C). When exposed to the flow, however, the deformation of *villin*$^{-/-}$ islet cells, but not their size, was reduced compared with that of *villin*$^{+/+}$ islet cells (Figure 3C,D). The greater stiffness of *villin*$^{-/-}$ islet cells supports the role of villin in the regulation of the actin cytoskeleton in these cells.

3.4. Acute depletion of *villin* impairs insulin release

Because *villin* is genetically linked to *Ica512*, which regulates SG exocytosis, we investigated whether *villin* affects insulin release. Intriguingly, isolated *villin*$^{-/-}$ and *villin*$^{+/+}$ islets were comparable in terms of insulin content (Supplementary Figure 4A), basal insulin secretion (Supplementary Figure 4B), and glucose-stimulated insulin secretion (Figure 4A). However, acute downregulation of villin expression by 60% in *villin*$^{+/+}$ islets (Figure 4B) reduced the insulin stimulation index (Figure 4C) but not insulin content (Supplementary
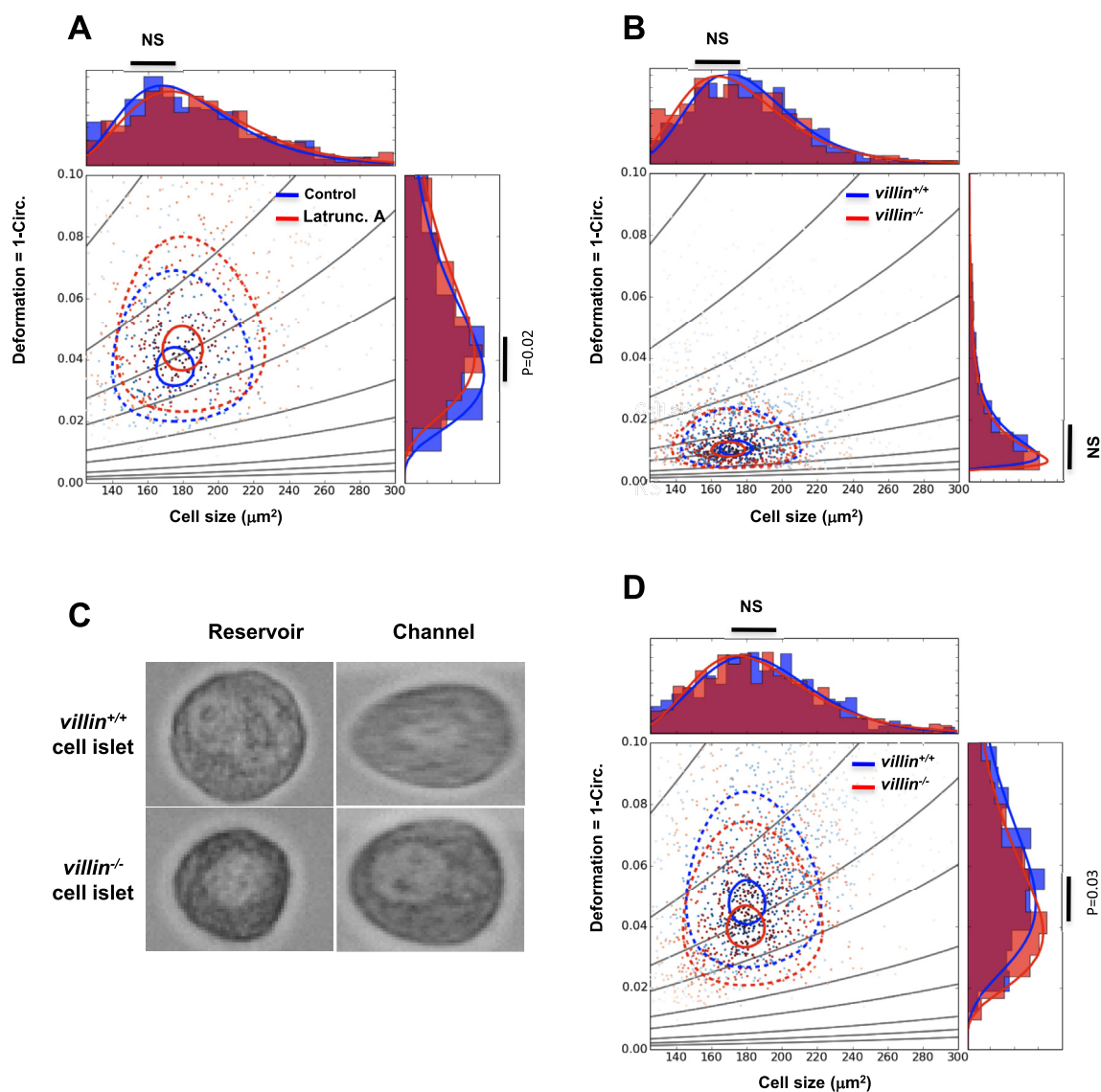

Figure 3: Deformability of *villin*$^{-/-}$ islets. (A) Deformability of mouse islets treated with or without latrunculin A (200 nM). **(B)** Deformation of *villin*$^{+/+}$ and *villin*$^{-/-}$ islets in the reservoir. **(C)** Images of single *villin*$^{+/+}$ and *villin*$^{-/-}$ islet cells in the reservoir or in the constricted channel of the microfluidic chamber. **(D)** Scatterplot of *villin*$^{+/+}$ and *villin*$^{-/-}$ islet cell deformation versus cell size. Contour lines representing 95% and 50% of the maximum cell density are shown as solid and dashed lines, respectively. The size distribution and deformability distribution are shown in the top and right panels, respectively, in **A**, **B**, and **D**.
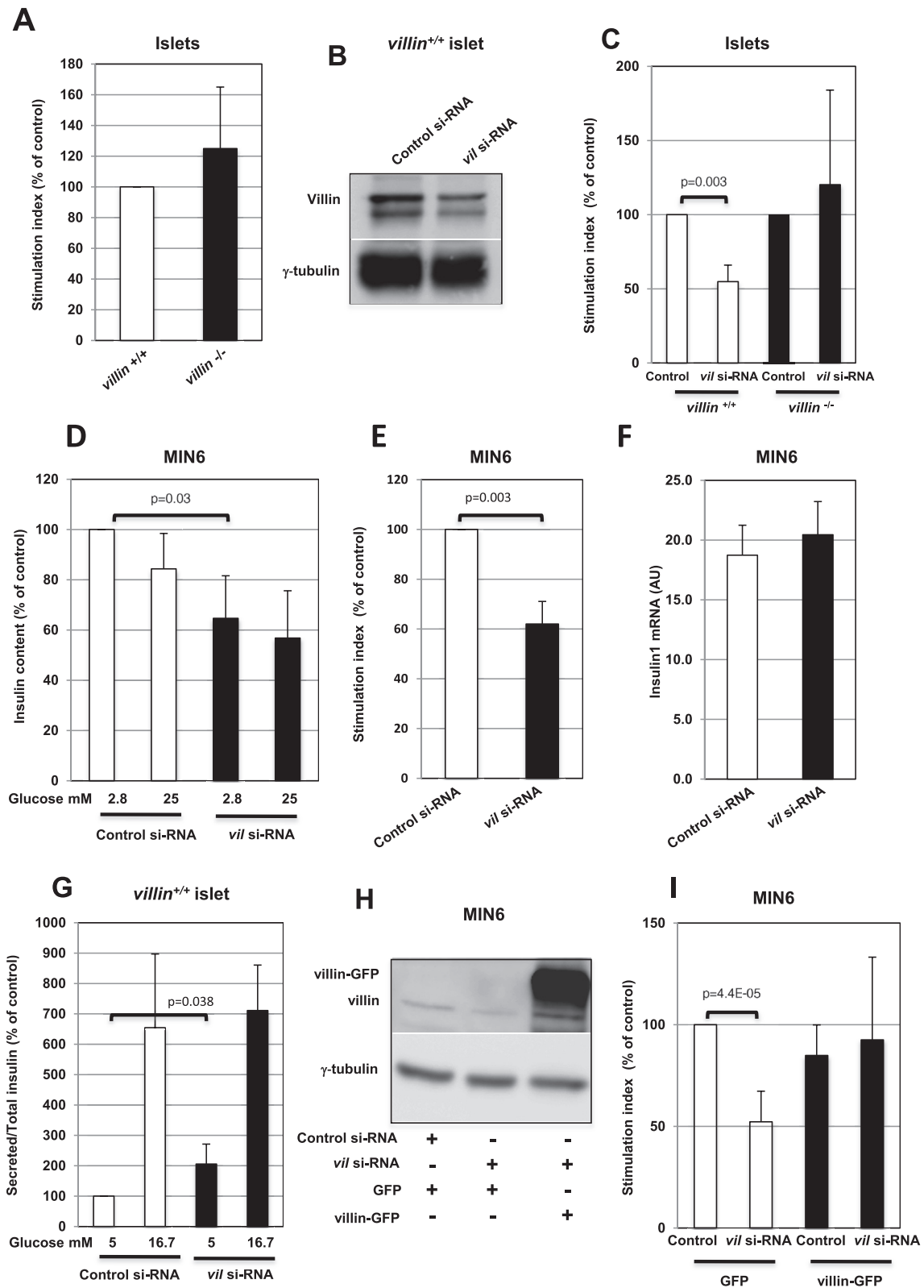
Figure 4: Insulin secretion is decreased in *villin*$^{-/-}$ islets and *villin*-depleted MIN6 cells. (A) Insulin stimulation index of *villin*$^{+/+}$ and *villin*$^{-/-}$ islets. (B) Immunoblots for villin and γ-tubulin in extracts of *villin*$^{+/+}$ islets treated with control or *villin* siRNA oligonucleotides. (C) Insulin stimulation index of *villin*$^{+/+}$ and *villin*$^{-/-}$ islets treated with control or *villin* siRNA oligonucleotides. (D—F) Insulin content at 2.8 and 25 mM glucose (D), stimulation index (E), and *insulin-1* mRNA expression (F) of control or *villin*-depleted MIN6 cells. (G) Basal and glucose-stimulated insulin secretion in *villin*$^{+/+}$ islets treated with control or *villin* siRNA oligonucleotides. (H) Immunoblotting for GFP and γ-tubulin in extracts of MIN6 cells transfected with GFP or villin-GFP and treated with control or *villin* siRNA oligonucleotides. (I) Insulin stimulation index of MIN6 cells transfected with GFP or villin-GFP and treated with control or *villin* siRNA oligonucleotides.

Figure 4C). The reduction in glucose-stimulated insulin release in *villin*-depleted islets was not due to the concomitant downregulation of off-target genes, because this deficit was not observed in *villin*$^{-/-}$ islets exposed to the same treatment (Figure 4C). Intestinal epithelial cells compensate for the lack of *villin* by functional redundancy with other actin binding proteins, especially plastin 1 and espin [34,35]. Likewise, we found that plastin was upregulated in *villin*$^{-/-}$ islets (Supplementary Figure 5A), but not in *villin*-depleted MIN6 or INS-1 cells (Supplementary Figure 5B and C). The insulin content (Figure 4D) as well as the levels of the SG cargo Ica512 (Supplementary Figure 4D) were reduced in villin-depleted MIN6 cells, which is compatible with a reduction of the SG stores. Moreover, stimulated insulin secretion (Figure 4E and Supplementary Figure 4E) was reduced in *villin*-depleted MIN6 cells while *insulin1* mRNA expression was unchanged (Figure 4F). Insulin content (Supplementary Figure 4F) and secretion (Supplementary Figure 4G,H) were also reduced in *villin*-depleted INS-1 cells. The reduced stimulation index in *villin*-depleted insulinoma cells was driven by the increased basal insulin release (Figure 4G, Supplementary Figure 4E,H), in line with the data mentioned above suggesting an increased consumption of the SG stores. Notably, expression of a villin-GFP chimera resistant to silencing in MIN6 cells (Figure 4H) restored the stimulation index, confirming that villin regulates insulin secretion (Figure 4I).

3.5. Villin regulates insulin granule dynamics
F-actin restrains SGs, partly via interactions between the actin binding complex β2-syntrophin/utrophin with Ica512 [9,10]. Therefore, we analyzed whether *villin* also regulates SG dynamics by using TIRFM in combination with MotionTracking/Kalaimoscope software [2,22] to automatically count cortical insulin SGs labeled with the fluorescent reporter Ins-SNAP$^{TMR-Star}$ and track their motion in living MIN6 cells co-transfected with GFP. As expected, stimulation of control GFP$^+$ MIN6 cells with 25 mM glucose, which promotes insulin release, reduced the density of cortical Ins-SNAP$^{TMR-Star+}$ SGs from 0.349 ± 0.042/μm^2 to 0.245 ± 0.007/μm^2 (Figure 5A). The density of Ins-SNAP$^{TMR-Star+}$ SGs was already reduced to 0.266 ± 0.017/μm^2 in *villin*-depleted GFP$^+$ MIN6 cells kept at rest with 2.8 mM glucose, and it was not decreased by glucose stimulation. Overexpression of villin-GFP restored the density of Ins-SNAP$^{TMR-Star+}$ SGs to 0.501 ± 0.014/μm^2 in resting *villin*-depleted MIN6 cells.

Glucose stimulation of control GFP$^+$ MIN6 cells increased the mean speed of processively moving Ins-SNAP$^{TMR-Star+}$ SGs from 0.43 ± 0.014 μm/s to 0.52 ± 0.015 μm/s (Figure 5B) and their track maximum displacement from 0.43 ± 0.015 μm to 0.51 ± 0.015 μm (Supplementary Figure 6A). Conversely, in resting *villin*-depleted GFP$^+$ MIN6 cells, the processive movement of Ins-SNAP$^{TMR-Star+}$ SGs displayed a mean speed of 0.50 ± 0.017 μm/s and track maximum displacement of 0.50 ± 0.016 μm. Both variables were unaffected by glucose stimulation with values of 0.54 ± 0.016 μm/s and 0.51 ± 0.017 μm, respectively. In line with these findings, glucose stimulation increased the collective diffusion coefficient (D) of Ins-SNAP$^{TMR-Star+}$ SGs in GFP$^+$ MIN6 cells but not in *villin*-depleted GFP$^+$ MIN6 cells (Figure 5C). Analysis of the mean square displacement (MSD) provided additional evidence for the increased mobility of SGs in *villin*-depleted MIN6 cells prior to glucose stimulation (Figure 5D). In control GFP$^+$ MIN6 cells, the MSD of Ins-SNAP$^{TMR-Star+}$ SGs increased linearly for ∼2 s before reaching a plateau — a motion that is characteristic of objects restricted within F-actin cages. Accordingly, glucose stimulation, which induces the remodeling of microfilaments, increased the MSD of Ins-SNAP$^{TMR-Star+}$ SGs for an extended period of time. Conversely, the MSD of SGs in *villin*-depleted cells did not vary

between the resting and stimulated conditions. The increasing noise of the tracks over time can be explained by the fewer SGs with long trajectories (Supplementary Figure 6B). This effect was more pronounced in *villin*-depleted cells compared to control cells, presumably because the efficiency of the knockdown varied among cells. Deconvolution of the MSD allowed us to classify the SGs into three dynamic components according to the previously defined D [13] as highly dynamic (D = ∼10^{-2} μm^2/s), restricted (D = ∼10^{-3} μm^2/s), and nearly immobile (D = ∼10^{-4} μm^2/s) (Figure 5E,F). This analysis revealed that the D of all three dynamic components was higher in resting, but not in stimulated, *villin*-depleted cells than in the corresponding control cells. Glucose stimulation increased the fraction of highly dynamic SGs from 10.8% ± 1.4% to 13.5% ± 1.1% (Figure 5G). In resting *villin*-depleted cells, highly dynamic SGs accounted for 15.0% ± 1.44% of the total number of SGs, and this pool was not increased by stimulation. The contribution of the other two dynamic components did not differ between control and *villin*-depleted cells at rest or after stimulation (Figure 5H,I).

3.6. Villin acts downstream of Ica512 in regulating SG dynamics and exocytosis
Finally, we investigated the interplay between villin and Ica512 in regulating SGs dynamics and exocytosis. To achieve this, we first estimated the size of the actin cages encasing cortical SGs based on the amplitude of the D of highly dynamic SGs. In control cells, the mean size of the actin cages increased in MIN6 cells from 0.82 μm at rest to 1.32 μm upon stimulation. The actin cages were enlarged in *villin*-depleted cells at rest to a mean size of 1.12 μm, which increased to 1.45 μm upon stimulation (Figure 6A). Enlarged actin cages were also present in resting *Ica512*-depleted cells (mean size 1.26 μm), but their size was not increased by stimulation (mean size 1.20 μm). These phenotypic changes were rescued by concomitant expression of villlin-GFP, which reduced the size of the actin cages at rest and induced greater remodeling of actin cages upon stimulation. The changes in the sizes of actin cages in resting cells and after remodeling upon stimulation were correlated with changes in the insulin stimulation index. Thus, larger cages in resting *villin*- or *Ica512*-depleted cells were coupled with a blunted stimulation index, presumably due to increased basal insulin release and thus exhaustion of SG stores, whereas expression of villin-GFP in *Ica512*-depleted cells normalized both the size of actin cages and the effects of glucose stimulation (Figure 6B). Taken together, these data indicate that villin regulates the cortical actin cytoskeleton downstream of Ica512 (Figure 6C).

4. DISCUSSION

In this study, we have shown that Ica512 regulates the expression of *villin* in mouse β cells. Villin belongs to the gelsolin protein family and is expressed in a few restricted tissues, being a major constituent of the actin bundles in the microvilli of intestinal and kidney epithelial cells, where it is involved in the absorptive and secretory function of epithelial cells by modulating F-actin polymerization/depolymerization. However, it is also expressed in cells lacking microvilli, such as interstinal crypt and M cells [reviewed in 33]. Pancreatic β cells have microvilli-like structures, which are poorly defined in terms of their function, but these structures are enriched with glucose transporter 2, by about 6-fold relative to other domains of the plasma membrane [36]. A recent proteomics study revealed that villin and its paralog gelsolin were upregulated in mouse islets stimulated *in vitro* with 16.7 mM glucose for 24 h, [37].
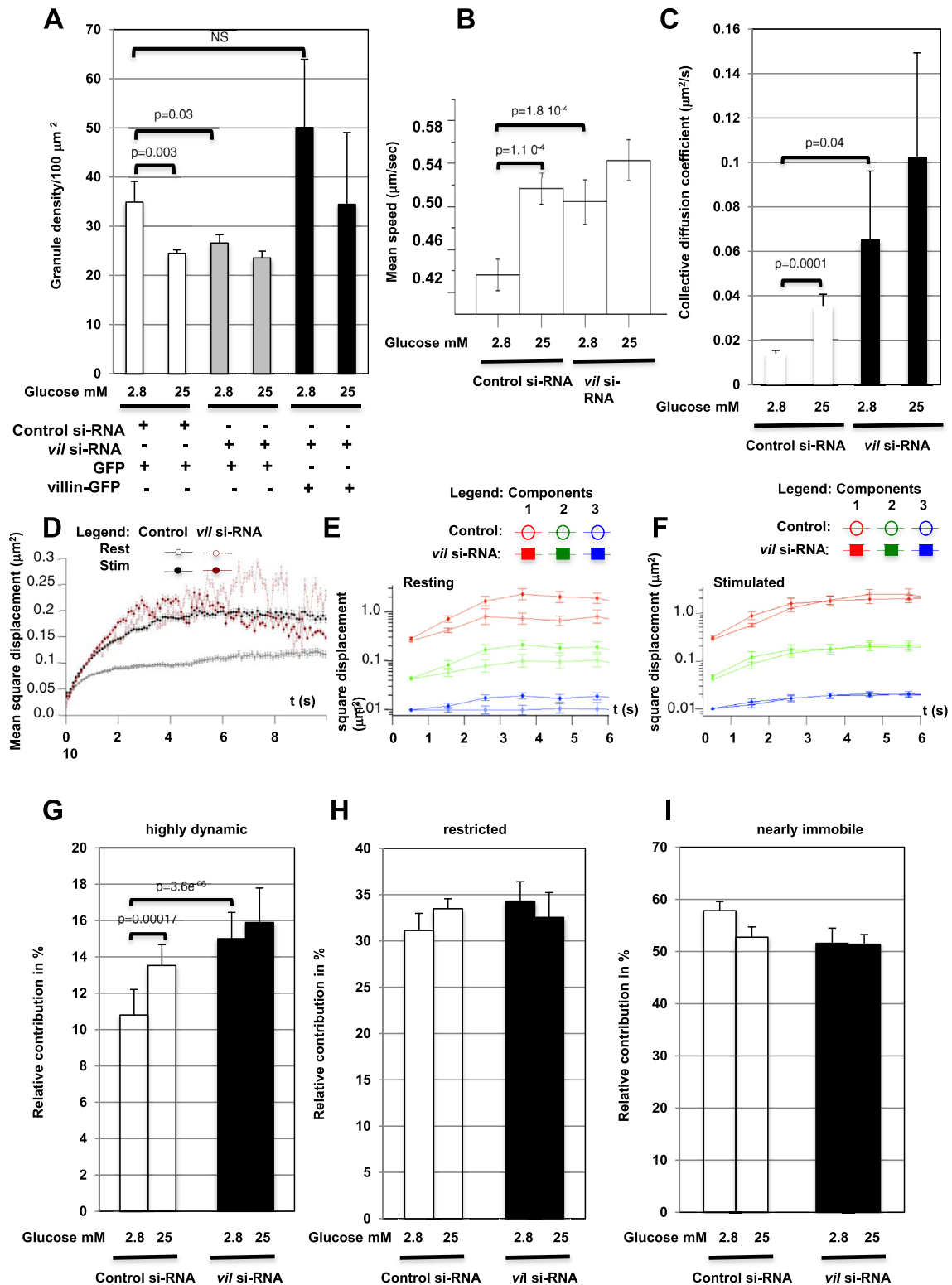
Figure 5: SG dynamics in *villin*-depleted MIN6. (A) Density of SGs in resting or glucose-stimulated MIN6 cells transfected with GFP or villin-GFP and treated with control or *villin* siRNA oligonucleotides. **(B–D)** Mean speed of processive SGs **(B)**, collective diffusion coefficient **(C)**, and mean square displacement of SGs **(D)** in resting or glucose-stimulated MIN6 cells transfected with GFP and treated with control or *villin* siRNA oligonucleotides. **(E,F)** Deconvolution in three dynamic components of the mean square displacement of SGs in resting **(E)** or glucose-stimulated **(F)** MIN6 cells transfected with GFP and treated with control or *villin* siRNA oligonucleotides. Highly dynamic SGs: red line; restricted SGs: green line; nearly immobile SGs: blue line. **(G–I)** Percentage of highly dynamic **(G)**, restricted **(H)**, and nearly immobile **(I)** SGs relative to the total number of tracked SGs in resting or glucose-stimulated MIN6 cells transfected with GFP and treated with control or *villin* siRNA oligonucleotides.
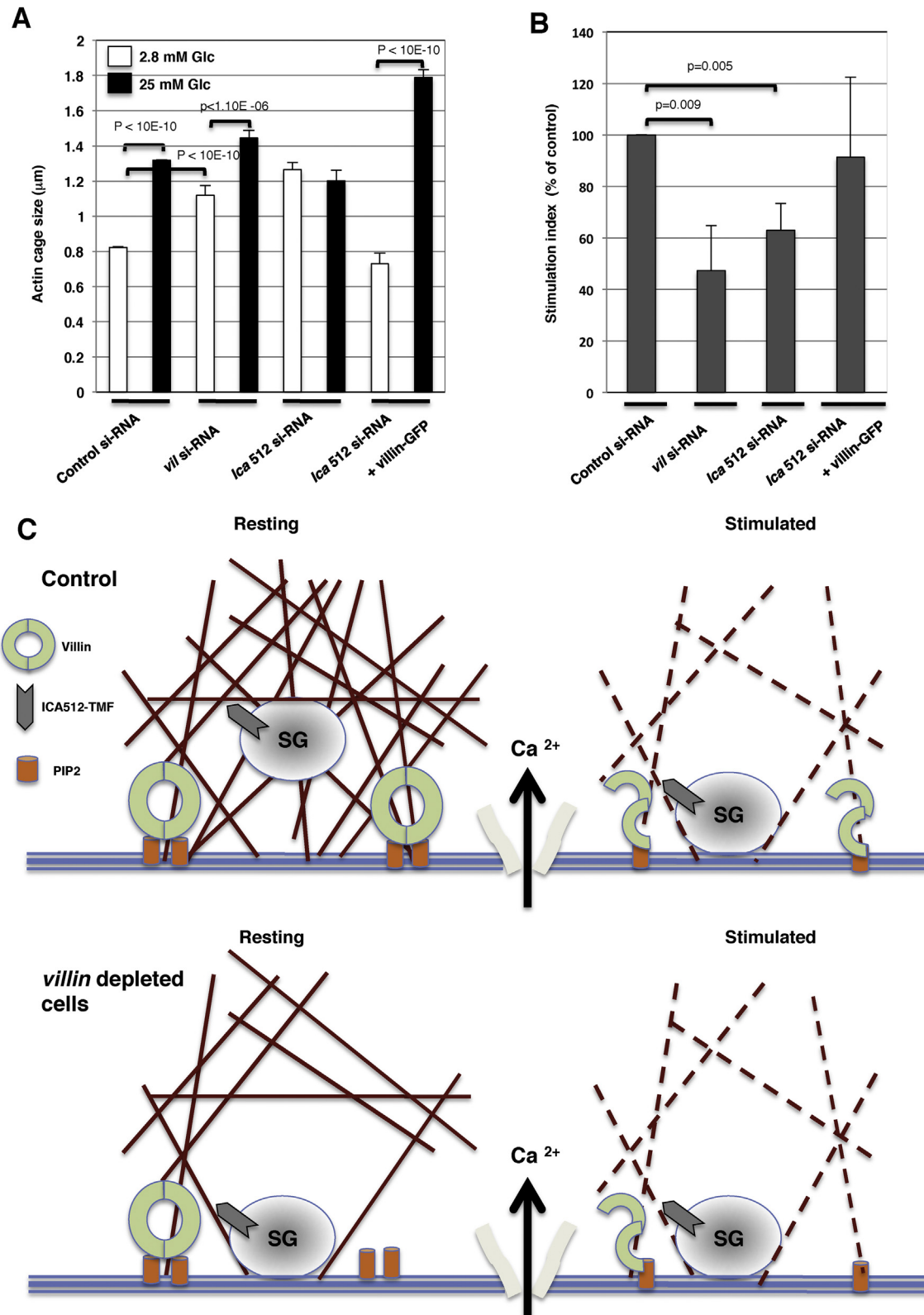
Figure 6: Altered actin cage size in *villin-* and *Ica512*-depleted MIN6 cells. (A,B) Actin cage size **(A)** and insulin stimulation index **(B)** in resting or glucose-stimulated MIN6 cells transfected with GFP or villin-GFP and treated with either control, *villin*, or *Ica512* siRNA oligonucleotides. **(C)** Remodeling of SG cages in *villin*^{+/+} and *villin*-depleted cells.

Here, we confirmed the expression of villin in pancreatic islets and verified its enrichment in the cellular cortex. Villin immunoreactivity was enhanced in insulinoma cells costimulated with high glucose and KCl to induce Ca^{2+} influx. Similar to gelsolin, villin is a globular protein that, in its autoinhibited configuration, bundles actin microfilaments [38]. This arrangement can be released via a "hinge mechanism" following an increase in the intracellular Ca^{2+} concentration. The resulting conformational change exposes the F-actin binding site of villin and regulates its actin-severing activity. To verify that villin controls the islet cell cytoskeleton, we compared the mechanical properties between $villin^{-/-}$ and $villin^{+/+}$ islets using high-throughput RT-DC. This is the first time RT-DC has been used for the analysis of islet cells, and allowed us to measure the changes in the shape and deformability of these cells. The evidence that $villin^{-/-}$ islet cells are less deformable than wild-type cells validates the role of villin in regulation of the islet cell cytoskeleton and agrees with the previous observation of the reduced migration of $villin^{-/-}$ epithelial cells [39]. This is in line with studies using differential centrifugation on extracts from $villin^{-/-}$ and $villin^{+/+}$ intestinal cells and confirmed the important role of villin is establishing the balance between polymerization and severing on actin filaments [40].

Although the mechanical properties of $villin^{-/-}$ islet cells are clearly altered compared with wild-type islet cells, there are few systemic metabolic changes in $villin^{-/-}$ mice. Specifically, glucose homeostasis of $villin^{-/-}$ mice was modestly improved compared with control littermates, conceivably due to a slight reduction in intestinal glucose absorption. This mild phenotype can be explained by the compensatory mechanism of plastin in $villin^{-/-}$ intestinal cells [34]. Indeed, glucose tolerance was improved in $villin^{-/-}$, $plastin^{-/-}$, and $espin^{-/-}$ mice [35].

The wide tissue distribution of villin precluded the use of $villin^{-/-}$ mice to assess its specific role in β cells. Therefore, we assessed glucose-stimulated insulin secretion using isolated $villin^{-/-}$ islets *in vitro* and also used isolated $villin^{+/+}$ islets and insulinoma cells in which *villin* expression had been acutely downregulated by RNAi. The insulin stimulation index of $villin^{-/-}$ islets was normal, possibly due to compensatory upregulation of plastin, but the insulin stimulation index was reduced in *villin*-depleted islets and insulinoma cells. Off-target effects were ruled out because the *villin* siRNAs did not affect insulin secretion in $villin^{-/-}$ islets and because the insulin stimulation index of insulinoma cells was rescued by concominant expression of RNAi-resistant villin-GFP. The decreased insulin stimulation index of *villin*-depleted β cells was driven by an increase in basal insulin secretion and a decrease in glucose-stimulated insulin release. Villin is not the first actin-severing protein to be implicated in insulin secretion. Studies in two MIN6 cell clones, which differed markedly in their secretory responses, showed that its paralogue gelsolin promotes insulin release via its Ca^{2+}-dependent F-actin severing and remodeling activity upon glucose stimulation [41]. Gelsolin was also shown to modulate insulin secretion via Ca^{2+}-regulated binding to syntaxin 4 [42] and to promote β cell survival [43]. Similarly, the Ca^{2+}-activated actin severing activity of scinderin was reported to promote regulated exocytosis of SGs in chromaffin cells [44].

"Leaky" basal insulin secretion in *villin*-depleted β cells could explain the lower density of SGs near the plasma membrane, a finding that was correlated with the greater mobility of SGs in conditions in which actin bundling is conceivably reduced. The processive motion of SGs was 21% faster, and the collective diffusion of SGs was 2.5 times greater in stimulated control cells than in the corresponding unstimulated cells. These findings are consistent with the notion that stimulation extends the excursions of SGs, enabling them to move to areas not previously visited in the last few hundred milliseconds before exocytosis [45,

reviewed in 46]. The processive motion and collective diffusion of SGs were 16% and 4.5 times greater, respectively, in resting *villin*-depleted cells than in resting control cells, but they were not increased further by glucose stimulation. Based on the MSD, we calculated that in resting control cells, SGs are confined within an area with a mean size of 0.82 μm, comparable to the estimated size of actin cages surrounding SGs in chromaffin cells [28,47]. *Villin*-depletion was associated with a significant enlargement of the actin cages in resting cells, similar to the effects of glucose stimulation did in control cells. A comparable increase in the size of actin cages was observed in resting *Ica512*-depleted cells, in which villin expression was also downregulated. Notably, this phenotype was rescued by villin-GFP overexpression. In other words, the actin cages in resting *Ica512*-depleted, villin-GFP$^+$ cells were similar in size to those in resting control cells. Moreover, the stimulation-induced expansion of actin cages was restored in villin-GFP$^+$ cells, conceivably due to villin Ca^{2+}-dependent actin-severing activity. These changes were accompanied by restoration of the insulin stimulation index relative to that in *villin*- or *Ica512*-depleted cells. Taken together, these findings suggest that villin acts downstream of Ica512 in regulating the mobility and access to the plasma membrane of SGs. However, since stimulation could promote the further enlargement of actin cages in *villin*-depleted, but not in *Ica512*-depleted cells, it seems likely that villin is not the only factor through which Ica512 regulates SG dynamics. One such factor could be β2-syntrophin, an adapter protein involved in the tethering of SGs to F-actin through Ica512 [10]. These considerations are in line with previous studies suggesting that neither Ica512/Ia-2 nor its paralogue Ia-2β/phogrin is indispensable for SG exocytosis but "that their absence facilitates the secretory response to the triggering Ca^{2+} signal, perhaps by suppressing the interaction with proteins [8,48] that impede rather than promote granule access to the exocytotic sites" [49].

The signaling pathway for regulation of *villin* expression by *Ica512* remains undefined. Intriguingly, *villin* expression is reduced in intestinal epithelial cells of Jak3$^{-/-}$ mice [50]. In rat β cells, cleavage of Ica512 intracellular domain upon SG exocytosis generates a cytosolic fragment that retrogradely enhances Jak/Stat activity in order to upregulate the transcription of SG cargoes, and thereby replenish SG stores [13,26]. Hence, in the future it will be interesting to establish whether Ica512 regulates *villin* expression through Stat signaling.

5. CONCLUSIONS

Our data indicate that villin is key for tight control of insulin SG mobility and exocytosis and that its expression is reduced upon deletion of the SG cargo protein Ica512. The genetic link between Ica512 and villin may therefore enable β cells to adjust the dimension of their F-actin cytoskeleton and its plasticity to the size of the SG stores.

AUTHORS' CONTRIBUTIONS

H.M. and M. S. designed the research and wrote the manuscript; H.M. performed most of the experimental work; B.M., P.H., A. I., and Y. K., contributed to the analysis of TIRF microscopic data; D. S. and T.H. performed transcriptomic analyses. M. H., O. O., and J.G. performed the RT-DC experiment; A. S. and C. M. provided technical assistance; J. D. and M. M.-H. contributed to data interpretation and modeling.

ACKNOWLEDGMENTS

CONFLICTS OF INTEREST

The authors declare that there are no conflicts of interest.

APPENDIX A. SUPPLEMENTARY DATA

Supplementary data related to this article can be found at http://dx.doi.org/10.1016/j.molmet.2016.05.015.

REFERENCES

[1] Sando, H., Borg, J., Steiner, D.F., 1972. Studies on the secretion of newly synthesized proinsulin and insulin from isolated rat islets of Langerhan. Journal of Clinical Investigation 51:1476—1485.

[2] Hoboth, P., Müller, A., Ivanova, A., Mziaut, H., Dehghany, J., Sönmez, A., et al., 2015. Aged insulin granules display reduced microtubule-dependent mobility and are disposed within actin-positive multigranular bodies. Proceedings of the National Academy of Sciences United States of America 112:667—676.

[3] Lelkes, P.I., Friedman, J.E., Rosenheck, K., Oplatka, A., 1986. Destabilization of actin filaments as a requirement for the secretion of catecholamines from permeabilized chromaffin cells. FEBS Letters 208:357—363.

[4] Muallem, S., Kwiatkowska, K., Xu, X., Yin, H.L., 1995. Actin filament disassembly is a sufficient final trigger for exocytosis in nonexcitable cells. Journal of Cell Biology 128:589—598.

[5] Borovikov, Y.S., Norman, J.C., Price, L.S., Weeds, A., Koffer, A., 1995. Secretion from permeabilised mast cells is enhanced by addition of gelsolin: contrasting effects of endogenous gelsolin. Journal of Cell Science 108:657—666.

[6] Henquin, J.C., Mourad, N.I., Nenquin, M., 2012. Disruption and stabilization of β-cell actin microfilaments differently influence insulin secretion triggered by intracellular Ca^{2+} mobilization or store-operated Ca^{2+}. FEBS Letters 586:89—95.

[7] Castellino, F., Heuser, J., Marchetti, S., Bruno, B., Luini, A., 1992. Glucocorticoid stabilization of actin filaments: a possible mechanism for inhibition of corticotropin release. Proceedings of the National Academy of Sciences United States of America 89:3775—3779.

[8] Ort, T., Voronov, S., Guo, J., Zawalich, K., Froehner, S.C., Zawalich, W., et al., 2001. Dephosphorylation of beta2-syntrophin and Ca2+/mu-calpain-mediated cleavage of Ica512 upon stimulation of insulin secretion. EMBO Journal 20:4013—4023.

[9] Trajkovski, M., Mziaut, H., Schubert, S., Kalaidzidis, Y., Altkrüger, A., Solimena, M., 2008. Regulation of insulin granule turnover in pancreatic beta-cells by cleaved ICA512. Journal of Biological Chemistry 283:33719—33729.

[10] Schubert, S., Knoch, K.P., Ouwendijk, J., Mohammed, S., Bodrov, Y., Jäger, M., et al., 2010. β2-Syntrophin is a Cdk5 substrate that restrains the motility of insulin secretory granules. PLoS One 5:e12929.

[11] Saeki, K., Zhu, M., Kubosaki, A., Xie, J., Lan, M.S., Notkins, A.L., 2002. Targeted disruption of the protein tyrosine phosphatase-like molecule IA-2 results in alterations in glucose tolerance tests and insulin secretion. Diabetes 51:1842—1850.

[12] Kubosaki, A., Gross, S., Miura, J., Saeki, K., Zhu, M., Nakamura, S., et al., 2004. Targeted disruption of the IA-2beta gene causes glucose intolerance and impairs insulin secretion but does not prevent the development of diabetes in NOD mice. Diabetes 53:1684—1691.

[13] Mziaut, H., Trajkovski, M., Kersting, S., Ehninger, A., Altkrüger, A., Lemaitre, R.P., et al., 2006. Synergy of glucose and growth hormone signalling in islet cells through ICA512 and STAT5. Nature Cell Biology 8:435—445.

[14] Ferrary, E., Cohen-Tannoudji, M., Pehau-Arnaudet, G., Lapillonne, A., Athman, R., Ruiz, T., et al., 1999. In vivo, villin is required for Ca(2+)-dependent F-actin disruption in intestinal brush borders. Journal of Cell Biology 146:819—830.

[15] Miyazaki, J., Araki, K., Yamato, E., Ikegami, H., Asano, T., Shibasaki, Y., et al., 1990. Establishment of a pancreatic beta cell line that retains glucose-inducible insulin secretion: special reference to expression of glucose transporter isoforms. Endocrinology 127:126—132.

[16] Asfari, M., Janjic, D., Meda, P., Li, G., Halban, P.A., Wollheim, C.B., 1992. Establishment of 2-mercaptoethanol-dependent differentiated insulin-secreting cell lines. Endocrinology 130:167—178.

[17] Behrendt, R., Schumann, T., Gerbaulet, A., Nguyen, L.A., Schubert, N., Alexopoulou, D., et al., 2013. Mouse SAMHD1 has antiretroviral activity and suppresses a spontaneous cell-intrinsic antiviral response. Cell Reports 4:689—696.

[18] Peters, D., Luo, X., Qiu, K., Liang, P., 2012. Speeding up large-scale next generation sequencing data analysis with pBWA. Journal of Biocomputing 1:1.

[19] Anders, S., Huber, W., 2010. Differential expression analysis for sequence count data. Genome Biology 11:R106.

[20] Benjamini, Y., Hochberg, Y., 1995. Controlling the false discovery rate: a practical and powerful approach to multiple testing. Journal of the Royal Statistical Society: Series B 57:289—300.

[21] Trajkovski, M., Mziaut, H., Altkrüger, A., Ouwendijk, J., Knoch, K.P., Müller, S., et al., 2004. Nuclear translocation of an ICA512 cytosolic fragment couples granule exocytosis and insulin expression in {beta}-cells. Journal of Cell Biology 167:1063—1074.

[22] Ivanova, A., Kalaidzidis, Y., Dirkx, R., Sarov, M., Gerlach, M., Schroth-Diez, B., et al., 2013. Age-dependent labeling and imaging of insulin secretory granules. Diabetes 62:3687—3696.

[23] Elbashir, S.M., Harborth, J., Lendeckel, W., Yalcin, A., Weber, K., Tuschl, T., 2001. Duplexes of 21-nucleotide RNAs mediate RNA interference in cultured mammalian cells. Nature 411:494—498.

[24] Knoch, K.P., Bergert, H., Borgonovo, B., Saeger, H.D., Altkrüger, A., Verkade, P., et al., 2004. Polypyrimidine tract-binding protein promotes insulin secretory granule biogenesis. Nature Cell Biology 6:207—214.

[25] Hermel, J.M., Dirkx Jr., R., Solimena, M., 1999. Post-translational modifications of ICA512, a receptor tyrosine phosphatase-like protein of secretory granules. European Journal of Neuroscience 11:2609—2620.

[26] Mziaut, H., Kersting, S., Knoch, K.P., Fan, W.H., Trajkovski, M., Erdmann, K., et al., 2008. ICA512 signaling enhances pancreatic beta-cell proliferation by regulating cyclins D through STATs. Proceedings of the National Academy of Sciences United States of America 105:674—679.

[27] Solimena, M., Dirkx Jr., R., Hermel, J.M., Pleasic-Williams, S., Shapiro, J.A., Caron, L., et al., 1996. ICA 512, an autoantigen of type I diabetes, is an intrinsic membrane protein of neurosecretory granule. EMBO Journal 15:2102—2114.

[28] Giner, D., López, I., Villanueva, J., Torres, V., Viniegra, S., Gutiérrez, L.M., 2007. Vesicle movements are governed by the size and dynamics of F-actin cytoskeletal structures in bovine chromaffin cells. Neuroscience 146:659—669.

[29] Wong, I.Y., Gardel, M.L., Reichman, D.R., Weeks, E.R., Valentine, M.T., Bausch, A.R., et al., 2004. Anomalous diffusion probes microstructure dynamics of entangled F-actin networks. Physical Reviews Letters 92:178101—178104.

Original article

[30] Fava, E., Dehghany, J., Ouwendijk, J., Müller, A., Niederlein, A., Verkade, P., et al., 2012. Novel standards in the measurement of rat insulin granules combining electron microscopy, high-content image analysis and in silico modelling. Diabetologia 55:1013—1023.

[31] Otto, O., Rosendahl, P., Mietke, A., Golfier, S., Herold, C., Klaue, D., et al., 2015. Real-time deformability cytometry: on-the-fly cell mechanical phenotyping. Nature Methods 12:199—202.

[32] Press, W.H., Teukolsky, S.A., Vetterling, W.T., Flannery, B.P., 2002. Numerical recipes in C. The art of scientific computing. Cambridge University Press chapter 6.4 (pp. 226—229) and chapter 14 (pp.609—655).

[33] Khurana, S., George, S.P., 2008. Regulation of cell structure and function by actin-binding proteins: villin's perspective. FEBS Letters 582:2128—2139.

[34] Grimm-Günter, E.M.S., Revenu, S., Ramos, S., Hurbain, I., Smyth, N., Ferrary, E., et al., 2009. Plastin 1 binds to keratin and is required for terminal web assembly in the intestinal. Molecular Biology of the Cell 20:2549—2562.

[35] Revenu, C., Ubelmann, F., Hurbain, I., El-Marjou, F., Dingli, F., Loew, D., et al., 2012. A new role for the architecture of microvillar actin bundles in apical retention of membrane proteins. Molecular Biology of the Cell 23:324—336.

[36] Orci, L., Thorens, B., Ravazzola, M., Lodish, H.F., 1989. Localization of the pancreatic beta cell glucose transporter to specific plasma membrane domains. Science 245:295—297.

[37] Waanders, L.F., Chwalek, K., Monetti, M., Kumar, C., Lammert, E., Mann, M., 2009. Quantitative proteomic analysis of single pancreatic islets. Proceedings of the National Academy of Sciences United States of America 106:18902—18907.

[38] Hesterberg, L.K., Weber, K., 1983. Demonstration of three distinct calcium-binding sites in villin, a modulator of actin assembly. Journal of Biological Chemistry 258:365—369.

[39] Ubelmann, F., Chamaillard, M., El-Marjou, F., Simon, A., Netter, J., Vignjevic, D., et al., 2013. Enterocyte loss of polarity and gut wound healing rely upon the F-actin-severing function of villin. PNAS 110:1380—1389.

[40] Lhocine, N., Arena, E.T., Bomme, P., Ubelmann, F., Prévost, M.C., Robine, S., et al., 2015. Apical invasion of intestinal epithelial cells by Salmonella typhimurium requires villin to remodel the brush border actin cytoskeleton. Cell Host Microbe 17:164—177.

[41] Tomas, A., Yermen, B., Min, L., Pessin, J.E., Halban, P.A., 2006. Regulation of pancreatic beta-cell insulin secretion by actin cytoskeleton remodelling: role of gelsolin and cooperation with the MAPK signalling pathway. Journal of Cell Science 119:2156—2167.

[42] Kalwat, M.A., Wiseman, D.A., Luo, W., Wang, Z., Thurmond, D.C., 2012. Gelsolin associates with the N terminus of syntaxin 4 to regulate insulin granule exocytosis. Molecular Endocrinology 26:128—141.

[43] Yermen, B., Tomas, A., Halban, P.A., 2007. Pro-survival role of gelsolin in mouse beta-cells. Diabetes 56:80—87.

[44] Zhang, L., Marcu, M.G., Nau-Staudt, K., Trifaró, J.M., 1995. Histamine-evoked chromaffin cell scinderin redistribution, F-actin disassembly, and secretion: in the absence of cortical F-actin disassembly, an increase in intracellular Ca^{2+} fails to trigger exocytosis. Journal of Neurochemistry 65:1297—1308.

[45] Degtyar, V.E., Allersma, M.W., Axelrod, D., Holz, R.W., 2007. Increased motion and travel, rather than stable docking, characterize the last moments before secretory granule fusion. Proceedings of the National Academy of Sciences United States of America 104:15929—15934.

[46] Holz, R.W., Axelrod, D., 2008. Secretory granule behaviour adjacent to the plasma membrane before and during exocytosis: total internal reflection fluorescence microscopy studies. Acta Physiologica (Oxford) 192:303—307.

[47] Torregrosa-Hetland, C.J., Villanueva, J., López-Font, I., Garcia-Martinez, V., Gil, A., Gonzalez Vélez, V., et al., 2010. Association of SNAREs and calcium channels with the borders of cytoskeletal cages organizes the secretory machinery in chromaffin cells. Molecular and Cellular Neurobiology 30:1315—1319.

[48] Hu, Y.F., Zhang, H.L., Cai, T., Harashima, S., Notkins, A.L., 2005. The IA-2 interactome. Diabetologia 48:2576—2581.

[49] Henquin, J.C., Nenquin, M., Szollosi, A., Kubosaki, A., Notkins, A.L., 2008. Insulin secretion in islets from mice with a double knockout for the dense core vesicle proteins islet antigen-2 (IA-2) and IA-2beta. Journal of Endocrinology 196:573—581.

[50] Mishra, J., Verma, R.K., Alpini, G., Meng, F., Kumar, N., 2013. Role of Janus kinase 3 in mucosal differentiation and predisposition to colitis. Journal of Biological Chemistry 288:31795—31806.